Broadband Emission from Spider Binaries

Zorawar Wadiasingh (NASA GSFC/USRA), Christian van der Merwe (NWU), Christo Venter (NWU), Alice Harding (LANL), Matthew Baring (Rice) and others

Fermi Symposium, April 17, 2021

Fermi LAT Discoveries - Black Widows and Redbacks

- **~100 millisecond pulsars discovered in unidentified Fermi LAT sources**
- **~20 black widows, ~9-10 redbacks (>60 known in other bands)**

Table 1
Measured and Derived Parameters of BW Pulsars

Name	P_{ms}	$\dot{P}_i$ (10^{-20})	L_{sd}[a] (10^{34} erg s^{-1})	B_8[b]	d (kpc)	P_b (hr)	M_{comp} ($M_\odot$)	a_{11}	E_{cut} (TeV)	References
J0023+0923[c]	3.05	1.15	2.50	4.88	0.7	3.3	0.016	1.01	2.40	(1)
J0610–2100[c]	3.86	0.34	0.36	2.96	3.5	6.9	0.025	1.65	3.04	(2)
J1124–3653[c]	2.41	0.57	2.50	3.05	1.7	5.4	0.027	1.40	2.03	(1)
J1301+0833[c]	1.84	0.95	9.36	3.44	0.7	6.5	0.024	1.59	1.37	(3)
J1311–3430[c]	2.56	2.08	7.64	6.01	1.4	1.56	0.008	0.61	2.33	(4)
J1446–4701[c]	2.19	1.01	5.93	3.88	1.5	6.7	0.019	1.62	1.52	(5)
J1544+4937[c]	2.16	0.31	1.87	2.12	1.2	2.8	0.018	0.91	2.72	(6)
J1731–1847	2.34	2.47	11.9	6.26	2.5	7.5	0.04	1.75	1.23	(7)
J1745+1017[c]	2.65	0.23	0.75	2.02	1.36	17.5	0.016	3.07	1.86	(8)
J1810+1744[c]	1.66	0.45	6.08	2.26	2	3.6	0.044	1.07	1.86	(1)
J1959+2048[c]	1.61	0.72	10.6	2.80	1.53	9.2	0.021	2.00	1.19	(9)
J2047+1053[c]	4.29	2.00	1.56	7.63	2	3	0.035	0.95	2.78	(3)
J2051–0827[c]	4.51	1.23	0.83	6.14	1	2.4	0.027	0.82	3.51	(2)
J2214+3000[c]	3.12	1.46	2.96	5.57	1.32	10	0.014	2.11	1.59	(10), (11)
J2234+0944[c]	3.63	1.94	2.50	6.91	1	10	0.015	2.11	1.66	(3), (5)
J2241–5236[c]	2.19	0.67	3.90	3.15	0.5	3.4	0.012	1.03	2.12	(12)
J2256–1024[c]	2.29	1.58	8.11	4.96	0.6	5.1	0.034	1.35	1.54	(1)

Table 2
Measured and Derived Parameters of RB Pulsars

Name	P_{ms}	$\dot{P}_i$ (10^{-20})	L_{sd}[a] (10^{34} erg s^{-1})	B_8[b]	d (kpc)	P_b (hr)	M_{comp} ($M_\odot$)	a_{11}	E_{cut} (TeV)	References
J1023+0038	1.69	1.20	15.4	3.72	0.6	4.8	0.2	1.33	1.33	(1)
J1628-3205	3.21	1.13	2.11	4.96	1.2	5	0.16	1.36	2.15	(2)
J1723-2837	1.86	0.75	7.18	3.08	0.75	14.8	0.4	2.90	1.09	(3), (4)
J1816+4510[c]	3.19	4.03	7.64	9.34	2.4	8.7	0.16	1.97	1.30	(5)
J2129-0429	7.61	43.54	6.08	47.4	0.9	15.2	0.37	2.94	1.12	(6)
J2215+5135[c]	2.61	2.79	9.67	7.03	3	4.2	0.22	1.22	1.55	(6)
J2339-0533[c]	2.88	1.39	3.59	5.21	0.4	4.6	0.26	1.30	1.93	(7), (8)

Venter et al. (2015)

Why are “Spider” Binaries Interesting?

- Clean systems: circular orbits, many orbits, pulsar well timed, companion radial velocities ==> inclination and component masses constrained
- Fermi gamma-ray pulsations — constrains pulsar magnetic obliquity and also binary inclination (if spin and orbital axes aligned)
- Many of them (~10 now with X-ray obs, ~60 in the radio) and growing
- Study shock acceleration and pulsar winds in oblique shocks
- Doppler boosting along shock necessary to match X-ray LCs. This constrains the character of the pulsar termination shock
- Target photons inverse Compton in the TeV
- Flares of the companion — u~1 to u >> 1 erg/cm^3 — well suited flaring timescales for IACTs
- SED should peak in the MeV — some (all?) are gamma-ray binaries
- Exciting for CTA and AMEGO (or any other sensitive MeV telescopes)

X-ray Observations

- Spectral photon indices are typically Γ ≈ 1-1.5 implying very hard underlying electron power-law distributions and efficient acceleration
- Up to 80 keV NuSTAR PL implies downstream shocked B ≳ 1 G by containment (Hillas criterion) arguments

J1023+0038 (rotation-powered state)
Tendulkar et al. (2014)

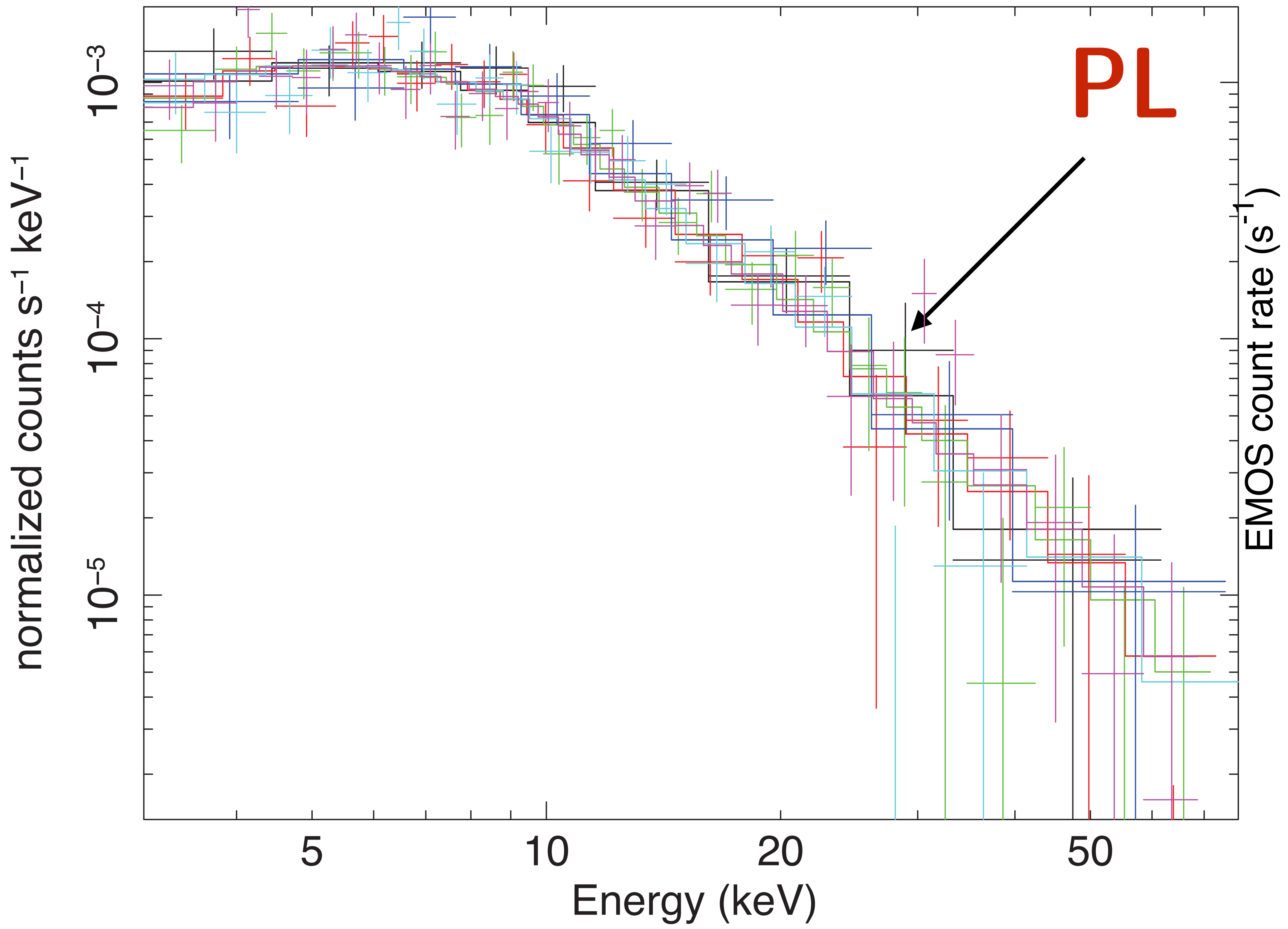

J1227-4853, de Martino et al. (2015)

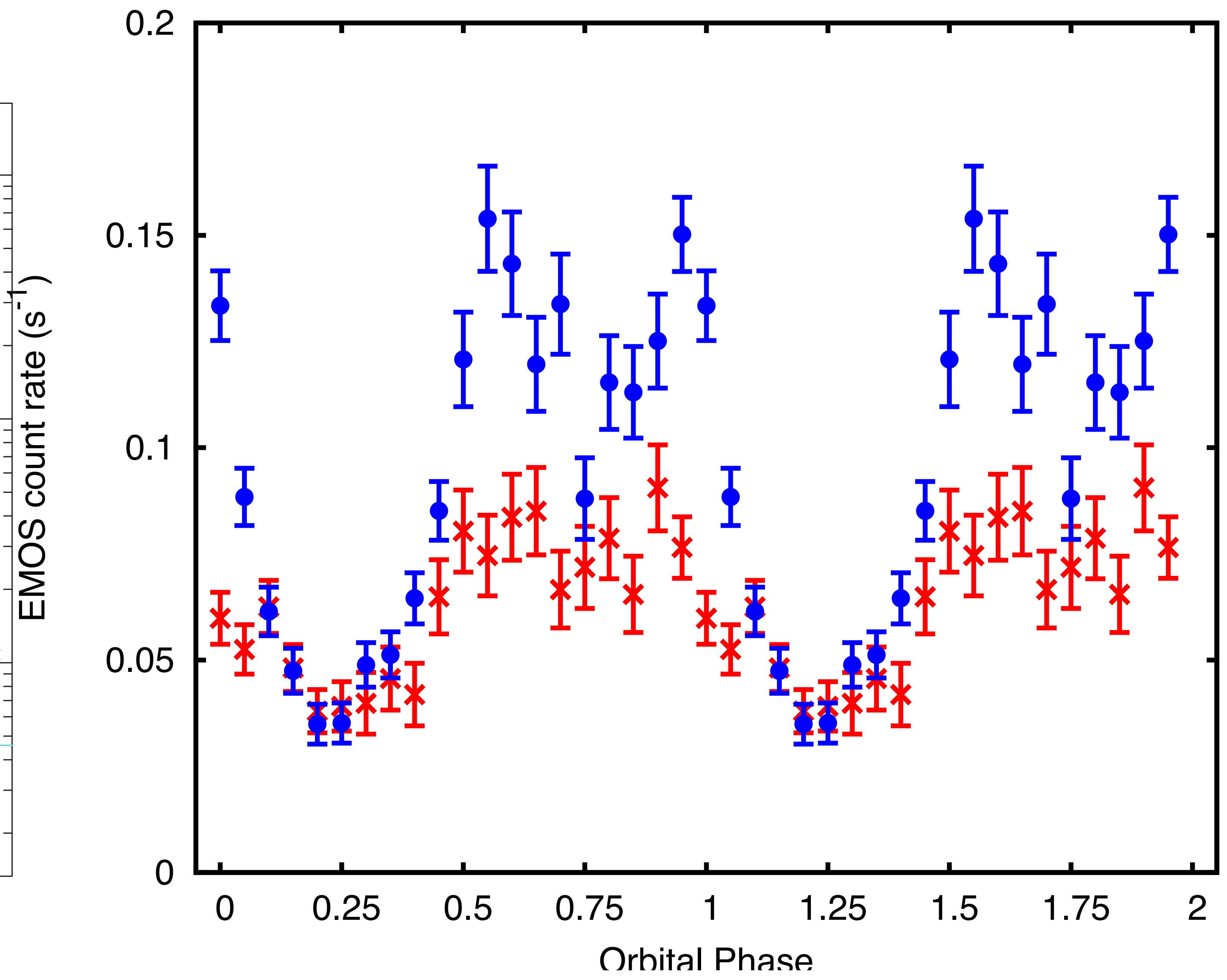

B1957+20, Huang et al. (2012)

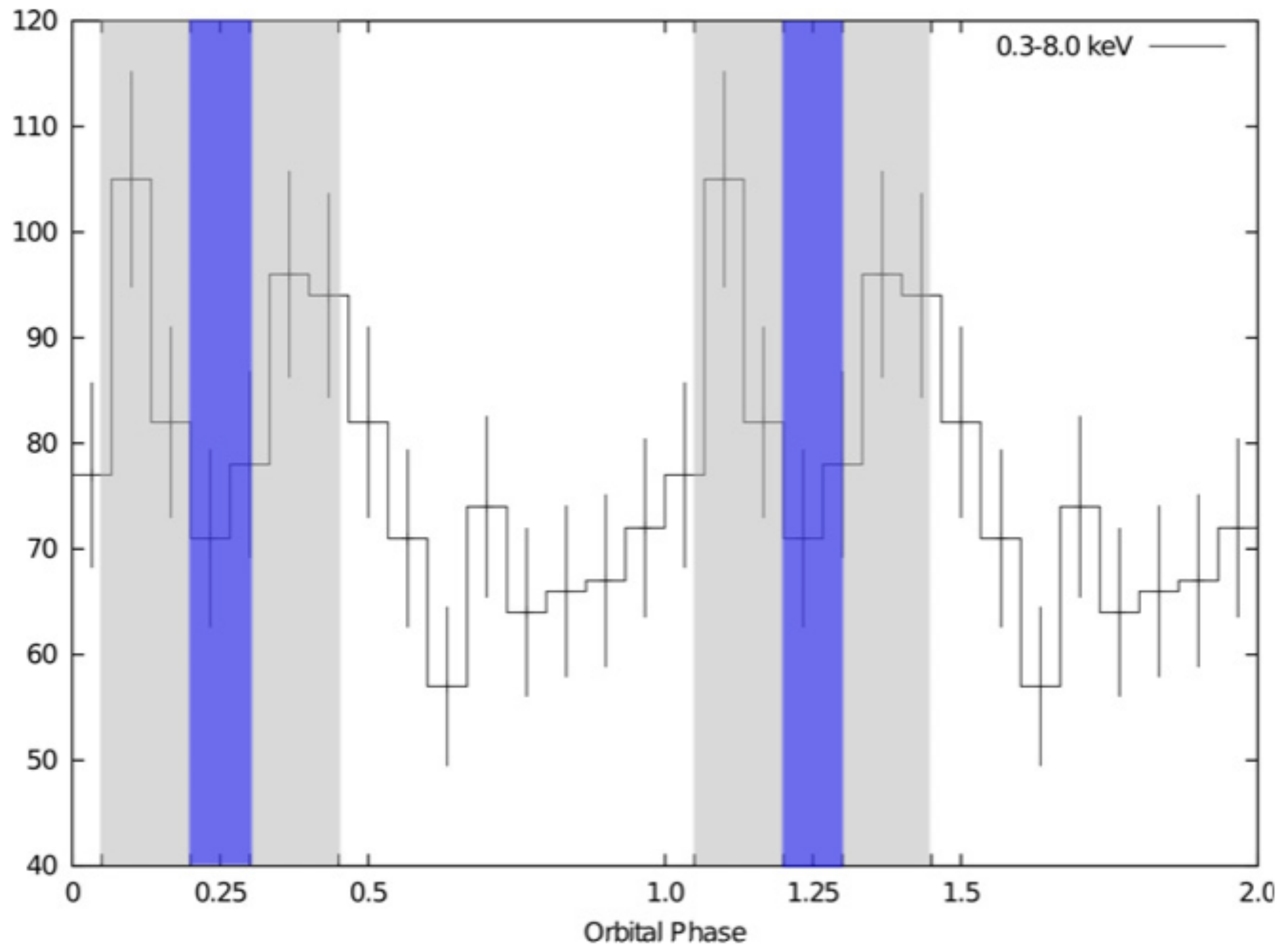

Geometric X-ray LC Fitting

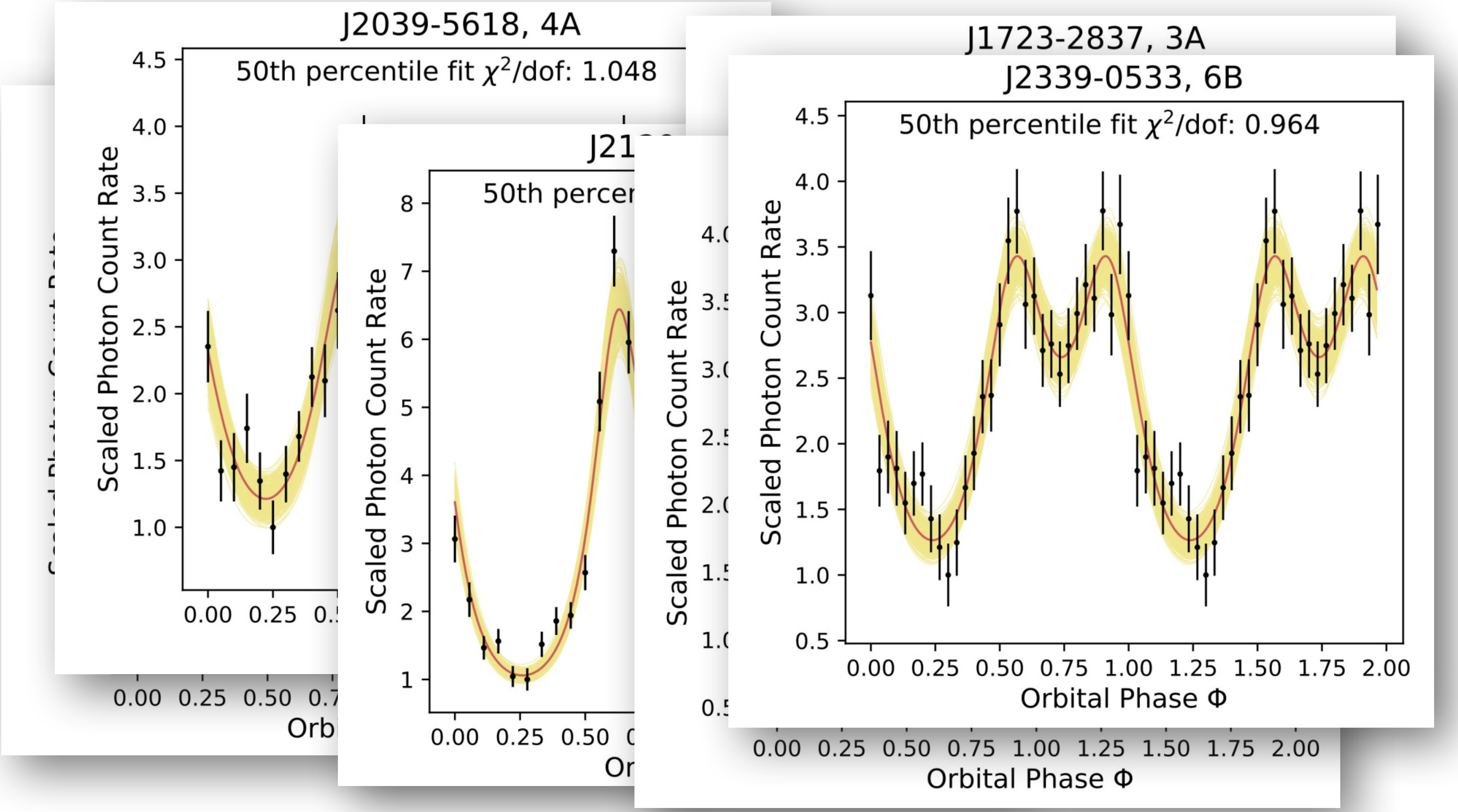

Wadiasingh et al., in prep.

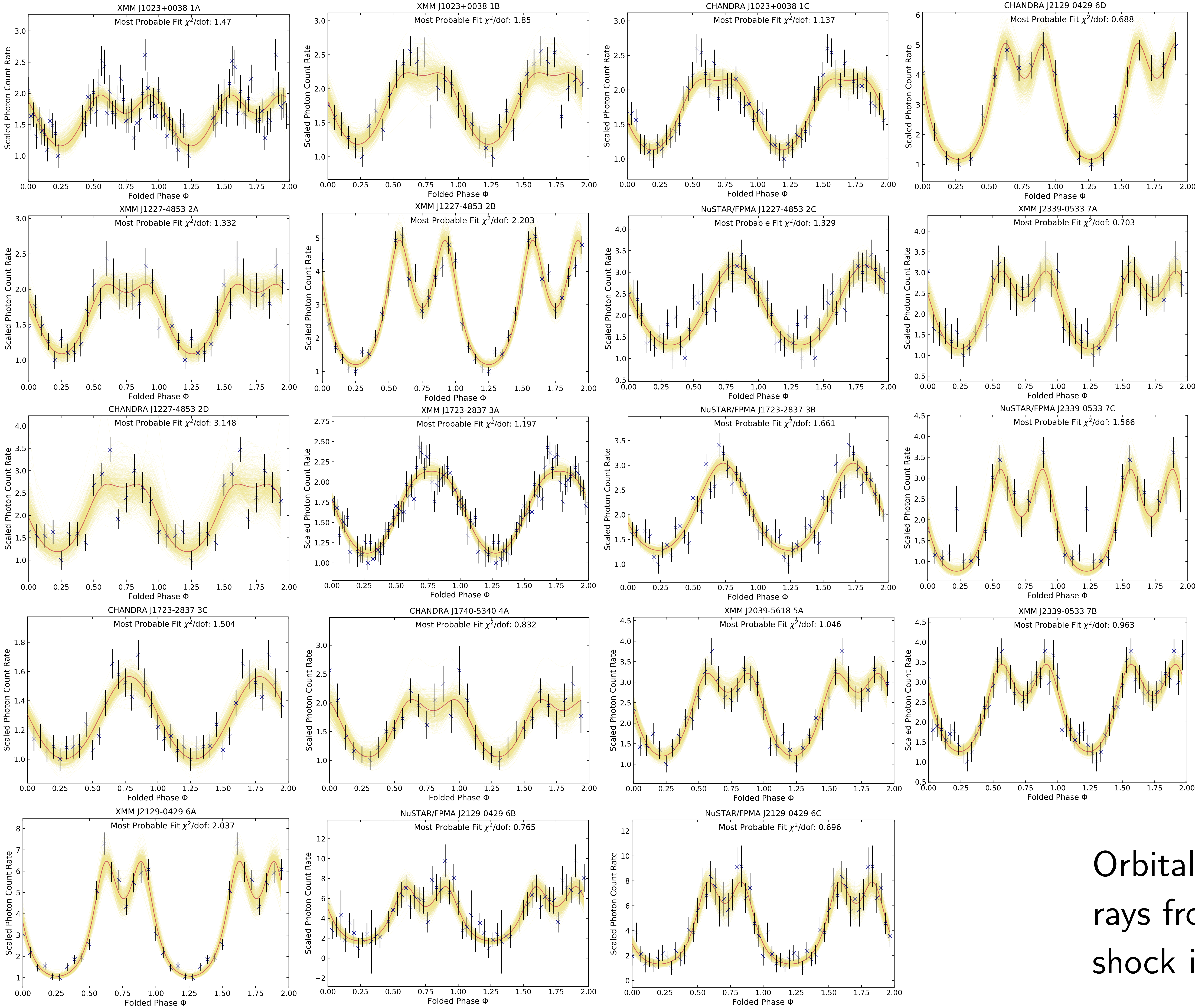

Orbital Modulation of X-rays from the intrabinary shock in redbacks

Schematic Geometry (Pulsar State)

Wadiasingh et al. (2017)

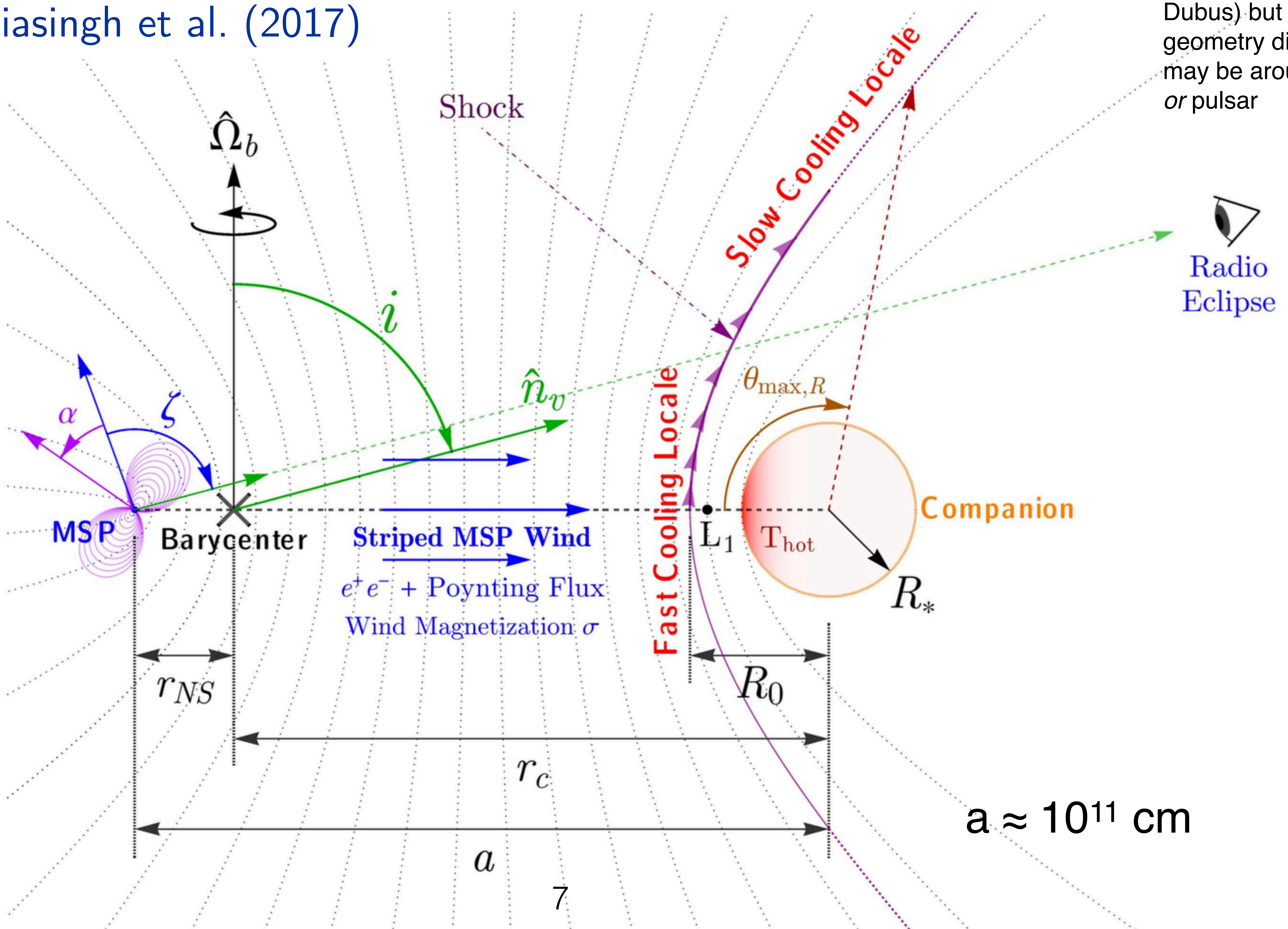

Physics somewhat similar to massive binaries (cf. Dubus) but scales and geometry differ — shock may be around companion *or* pulsar

$a \approx 10^{11}$ cm

Model Schematic — Doppler Boosting

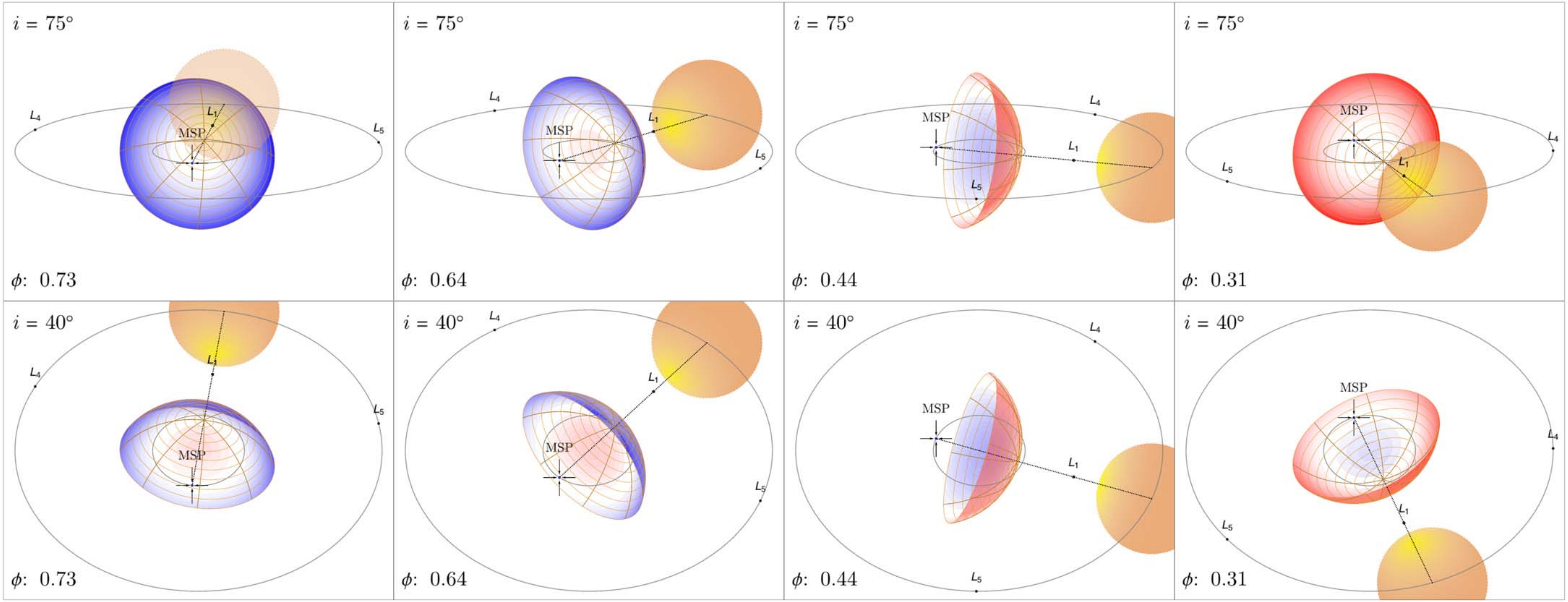

Van der Merwe, Wadiasingh, Venter, Harding & Baring;
ApJ 904:91, 2020

Pulsar Wind + companion B

$\alpha = 15°$

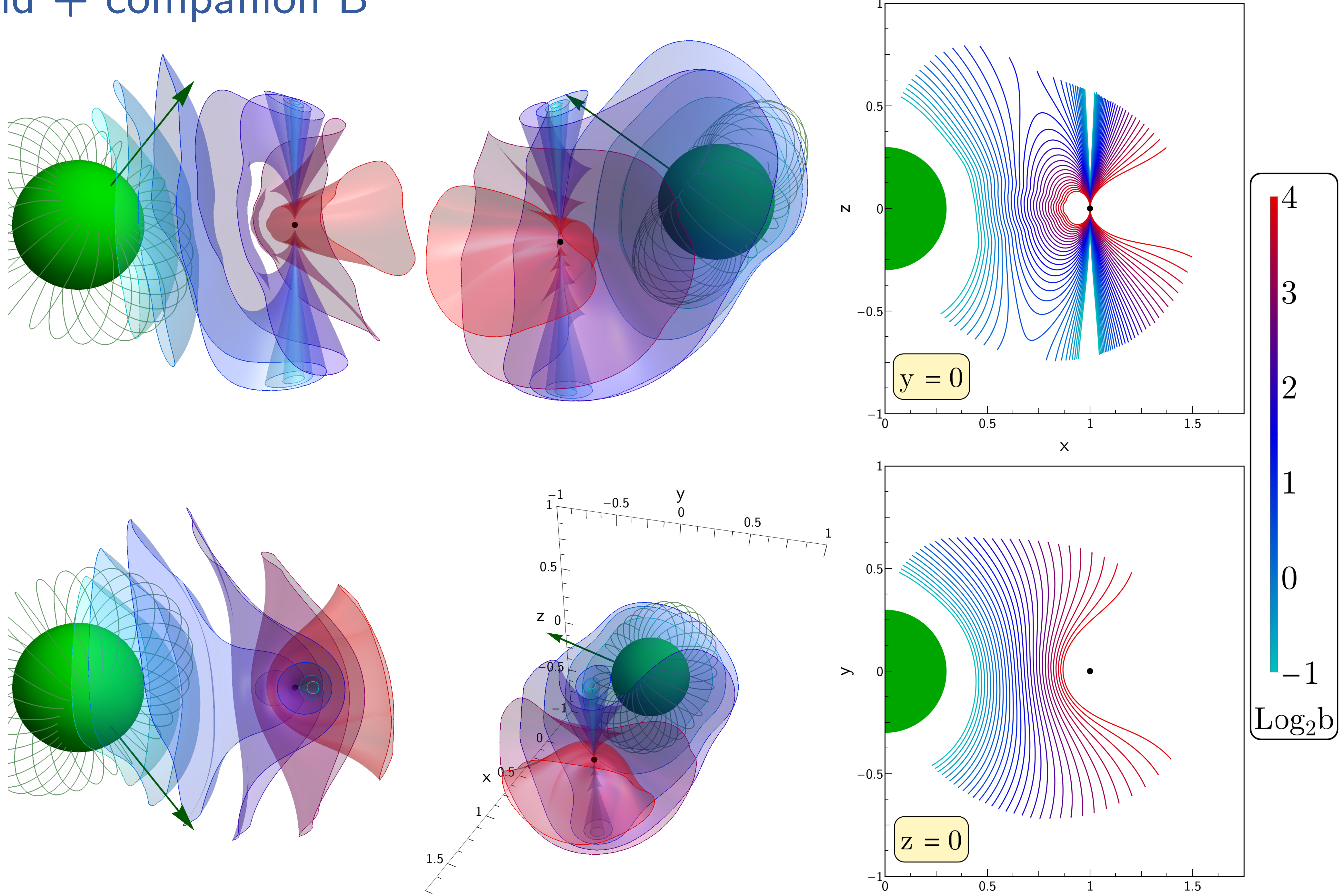

Wadiasingh et al. (2018)

Pulsar Wind + companion B

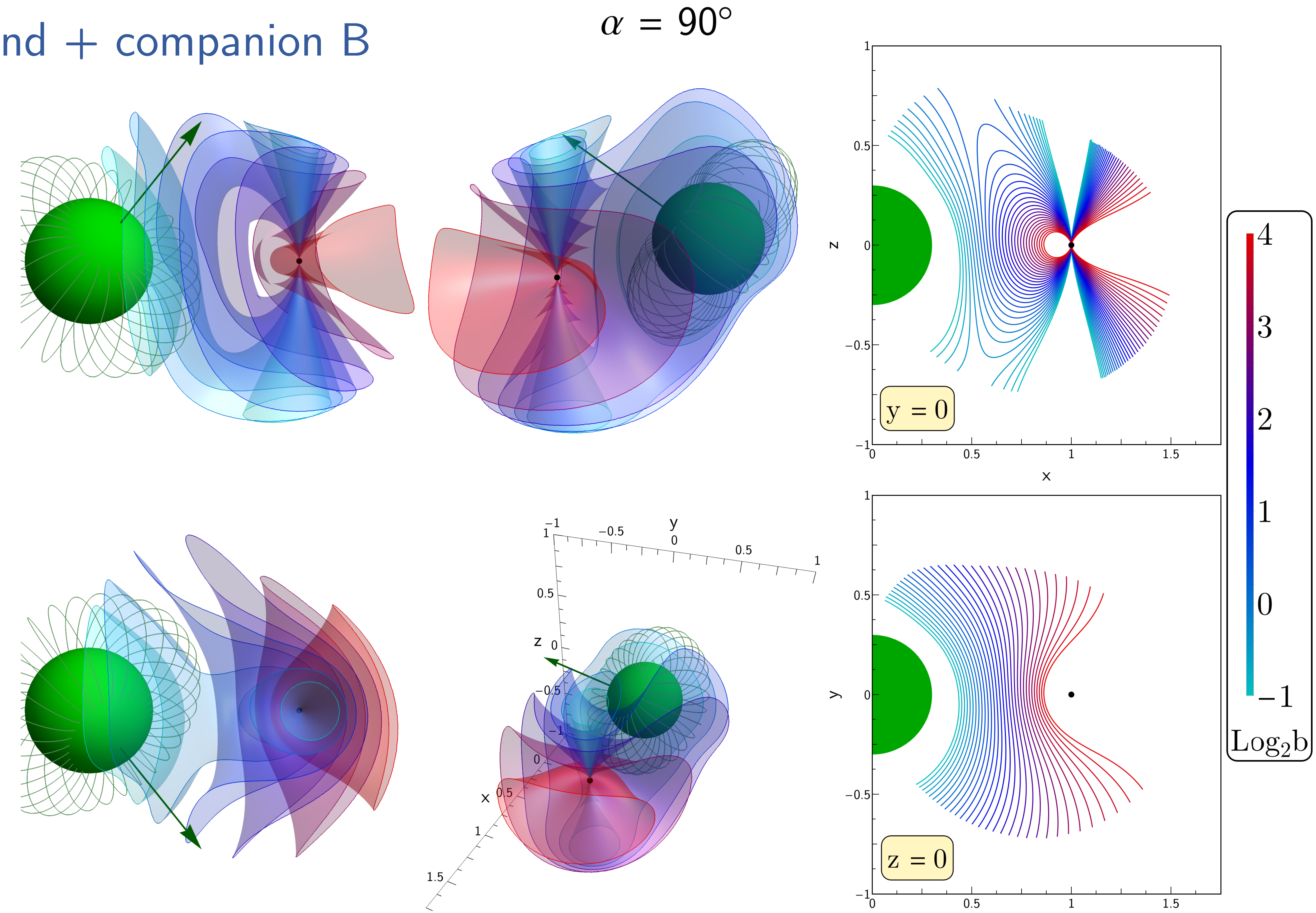

Wadiasingh et al. (2018)

Pulsar Wind
+
companion
B

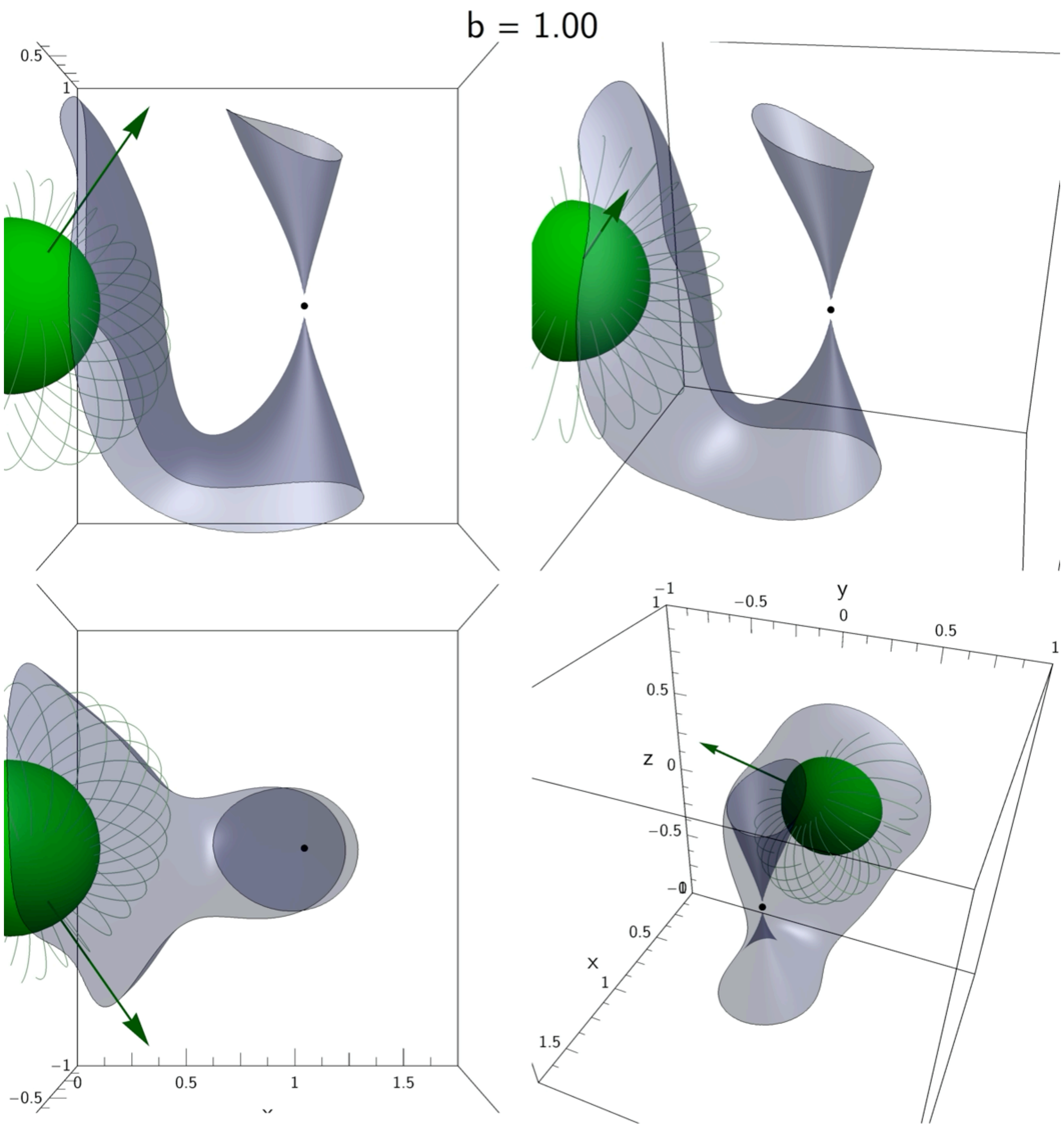

Fermi-LAT Orbital Modulation

Seen in a small subset of spiders

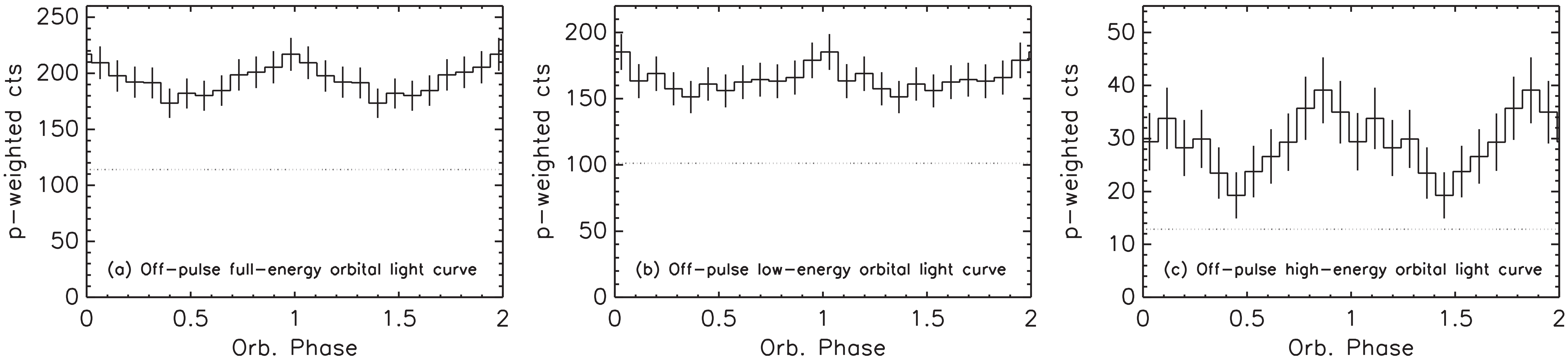

Black widow
J1311−3430

An et al. 2017

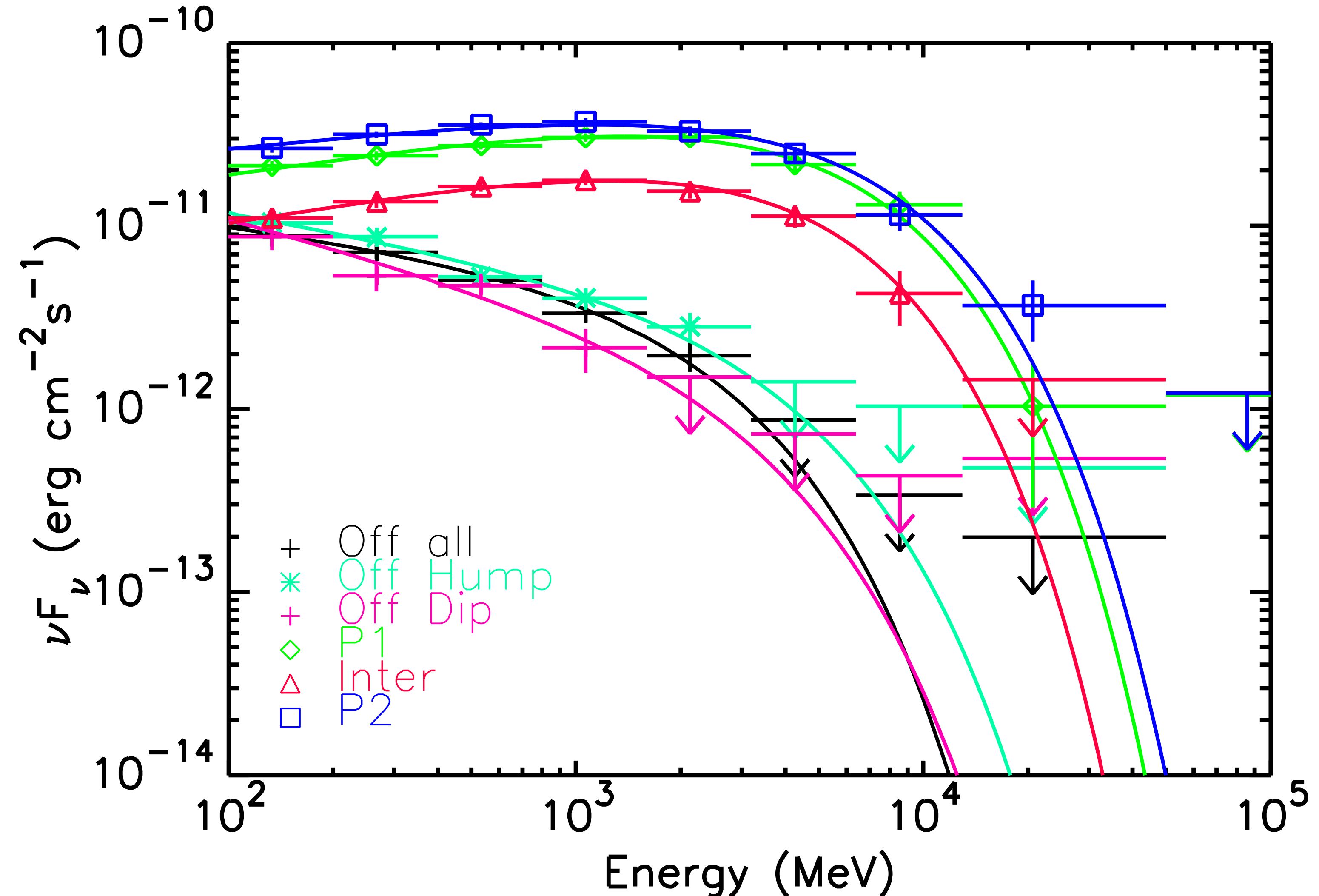

Peaks near
pulsar inferior
conjunction

Fermi-LAT Orbital Modulation — Pulse Enhancement

Redback J2039−5617

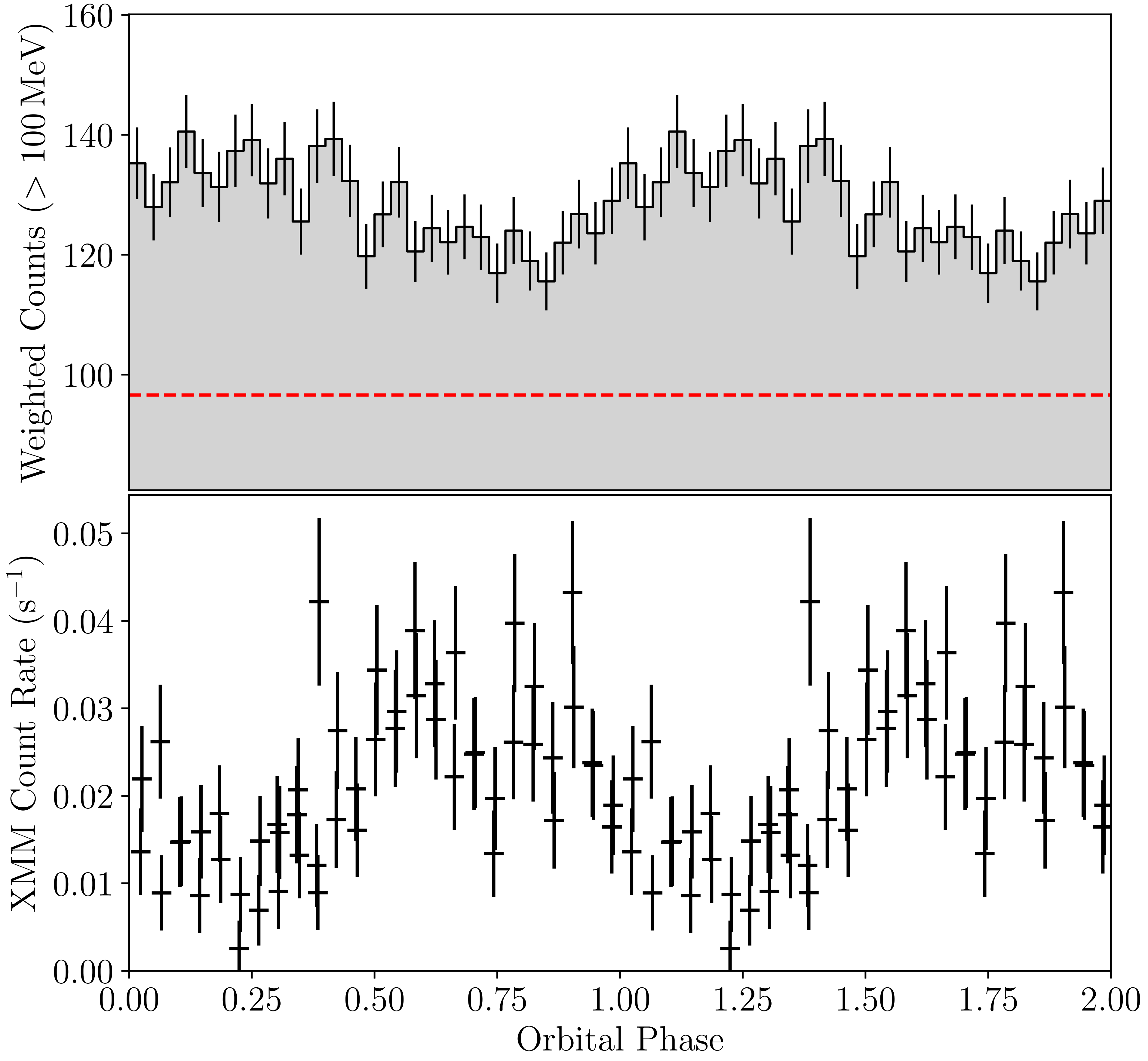

Clark et al. (2021)

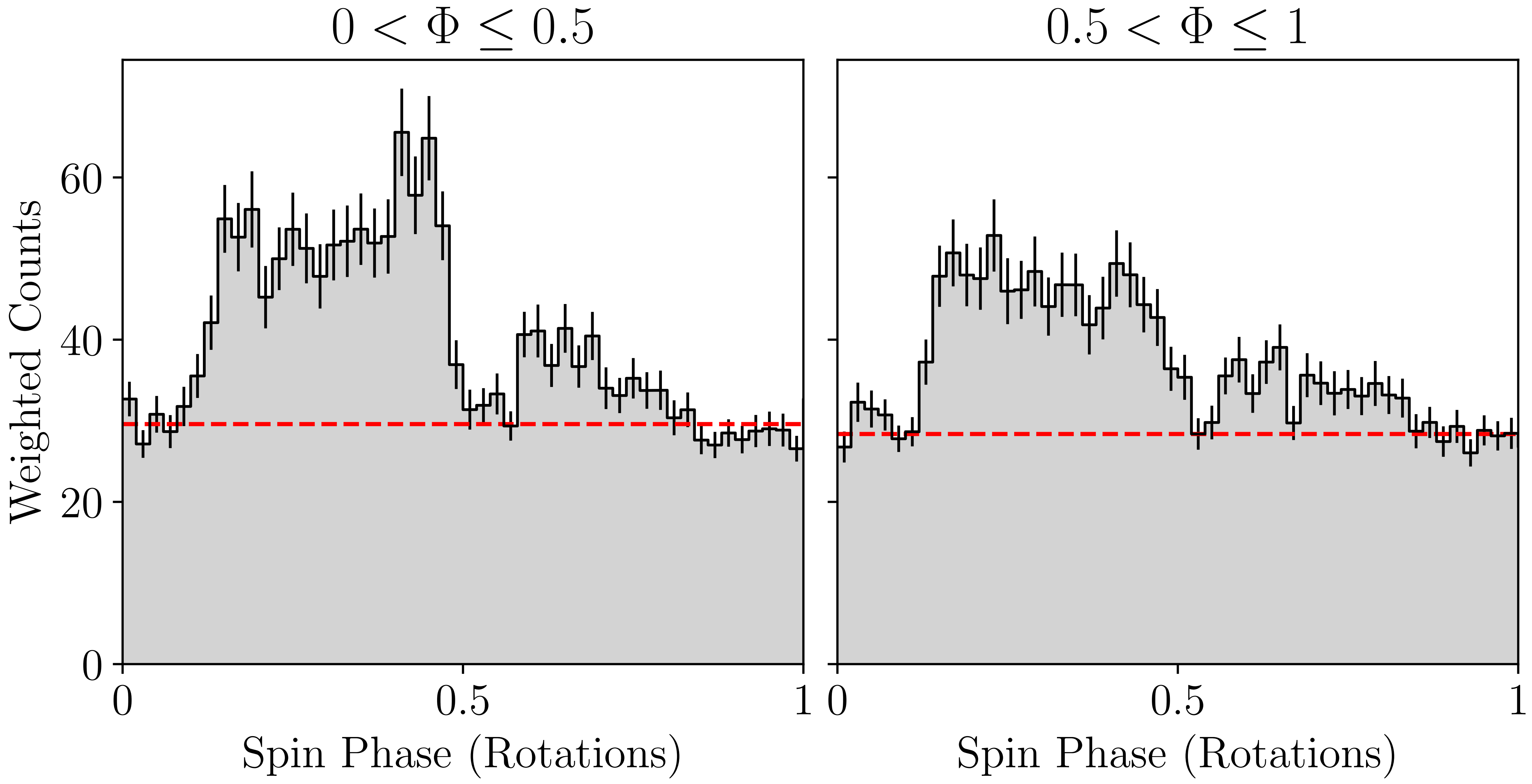

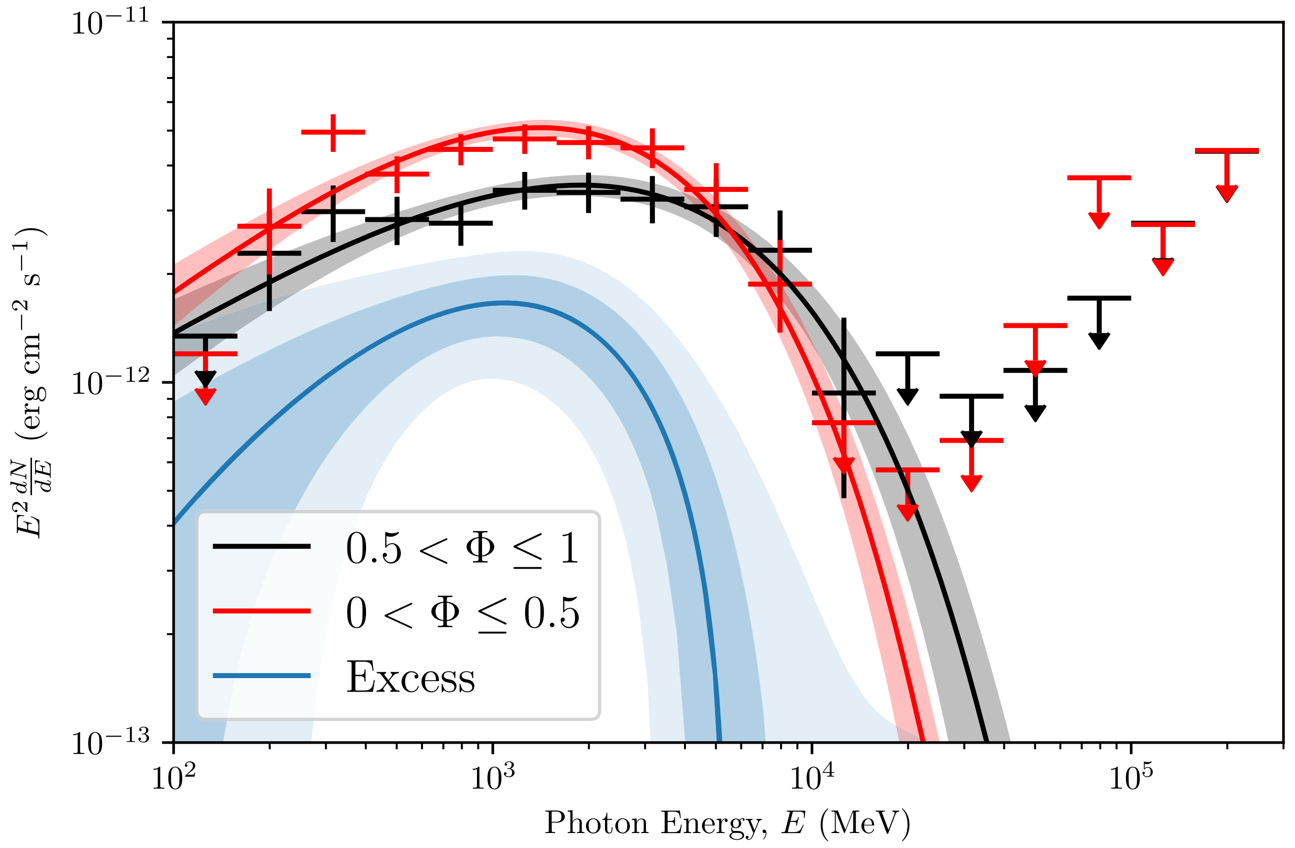

Pulsed enhancement near pulsar superior conjunction

Multizone Modeling — Simultaneous spectra and light curves

Van der Merwe, Wadiasingh, Venter, Harding and Baring; ApJ 904:91, 2020

Characteristic Scales

$$a \sim 10^{11} \text{ cm} \qquad R_* \sim 0.3a \qquad r_{\rm LC} \sim 10^7 \text{ cm} \sim 10^{-4} a$$

$$T_{\rm comp} \sim 5000 - 8000 \text{ K}$$

$$B_{\rm w} \approx \left(\frac{3\dot{E}_{\rm SD}}{2c}\right)^{1/2} \frac{1}{r_{\rm s}} = 22 \left(\frac{\dot{E}_{\rm SD}}{10^{35} \text{ erg s}^{-1}}\right)^{1/2} \left(\frac{10^{11} \text{ cm}}{r_{\rm s}}\right) \text{ G} \qquad B_{\rm s} \gtrsim B_{\rm s,min} \approx 4.4\, \epsilon_{X,\max}^{1/3} \left(\frac{10^9 \text{ cm}}{r_{\rm L}}\right)^{2/3} \text{ G}$$

$$\sigma \sim 10^{-3} - 10^{-2} \text{ from SED fitting}$$

$$u_B \sim \mathcal{O}(0.1 - 10) \text{ erg cm}^{-3}$$

$$u_{\rm ph} \sim \mathcal{O}(0.1 - 1) \text{ erg cm}^{-3}$$

$$E_{\rm cut} \sim 0.1 - 10 \text{ erg} \rightarrow 0.1 - 10 \text{ TeV electrons}$$

Simultaneous Spectra and Orbital Light Curves: Particle Injection and Transport + Beaming and Emission Code in Multiple Zones

Model Assumptions — `UMBRELA` Code

1. Hemispherical polar cap shape for shock surrounding companion (to be relaxed soon).
2. Azimuthal symmetry about line joining pulsar and companion $(d/d\phi = 0)$.
3. Steady-state $(d/dt = 0)$.
4. Isotropic black-body emission at temperature T from companion. IC on companion photons dominates at TeV. SSC is negligible.
5. Approximate particle transport using timescales (linearization).
6. Isotropic steady-state particle spectrum in comoving frame.
7. Bulk flow: linear profile for $\beta\Gamma(\theta)$ (bulk momentum linearly increasing).
8. $\tau_{\gamma\gamma}$ is quite small, even for flaring companions and is neglected for now.

Injection Spectrum

Cut-off Energy:

This is usually the minimum and sets Ecut

$$E_{\mathrm{cut}} = \min\{E_{\mathrm{SR\ RRLA}}, E_{\mathrm{Hillas}}, E_{\mathrm{MSP\ \Phi}}\}$$

Solid Angle & Diffusion:

$$Q_{\mathrm{PSR}}(E_{\mathrm{e}}) = Q_0 E_{\mathrm{e}}^{-\Gamma} \exp\left(-\frac{E_{\mathrm{e}}}{E_{\mathrm{cut}}}\right)$$

$$Q_1 = \left(\frac{1}{4\pi}\int_0^{2\pi}\int_{\lambda_1}^{\lambda_2} \sin\lambda\, d\lambda\, d\phi\right) Q_{\mathrm{PSR}} = \frac{1}{2}\left(\cos\lambda_1 - \cos\lambda_2\right) Q_{\mathrm{PSR}}$$

$$Q_i = \frac{1}{t_{\mathrm{diff}}}\frac{dN_{\mathrm{e},i-1}}{dE_{\mathrm{e}}} + \frac{1}{2}\left(\cos\lambda_i - \cos\lambda_{i+1}\right) Q_{\mathrm{PSR}}, \quad i > 1$$

Normalisation - Current and Energetics:

$$\dot{N}_{\mathrm{GJ}} = \frac{B_{\mathrm{PSR}} 4\pi^2 R_{\mathrm{PSR}}^3}{2ceP^2} \qquad \dot{N}_{\mathrm{II}} = M_{\pm}\dot{N}_{\mathrm{GJ}}$$

$$\int_{E_{\mathrm{min}}}^{\infty} Q_{\mathrm{PSR}}\, dE_{\mathrm{e}} = (M_{\pm}+1)\dot{N}_{\mathrm{GJ}} \qquad \int_{E_{\mathrm{min}}}^{\infty} E_{\mathrm{e}} Q_{\mathrm{PSR}}\, dE_{\mathrm{e}} = \eta_{\mathrm{p}}\dot{E}_{\mathrm{rot}}$$

Model Schematic

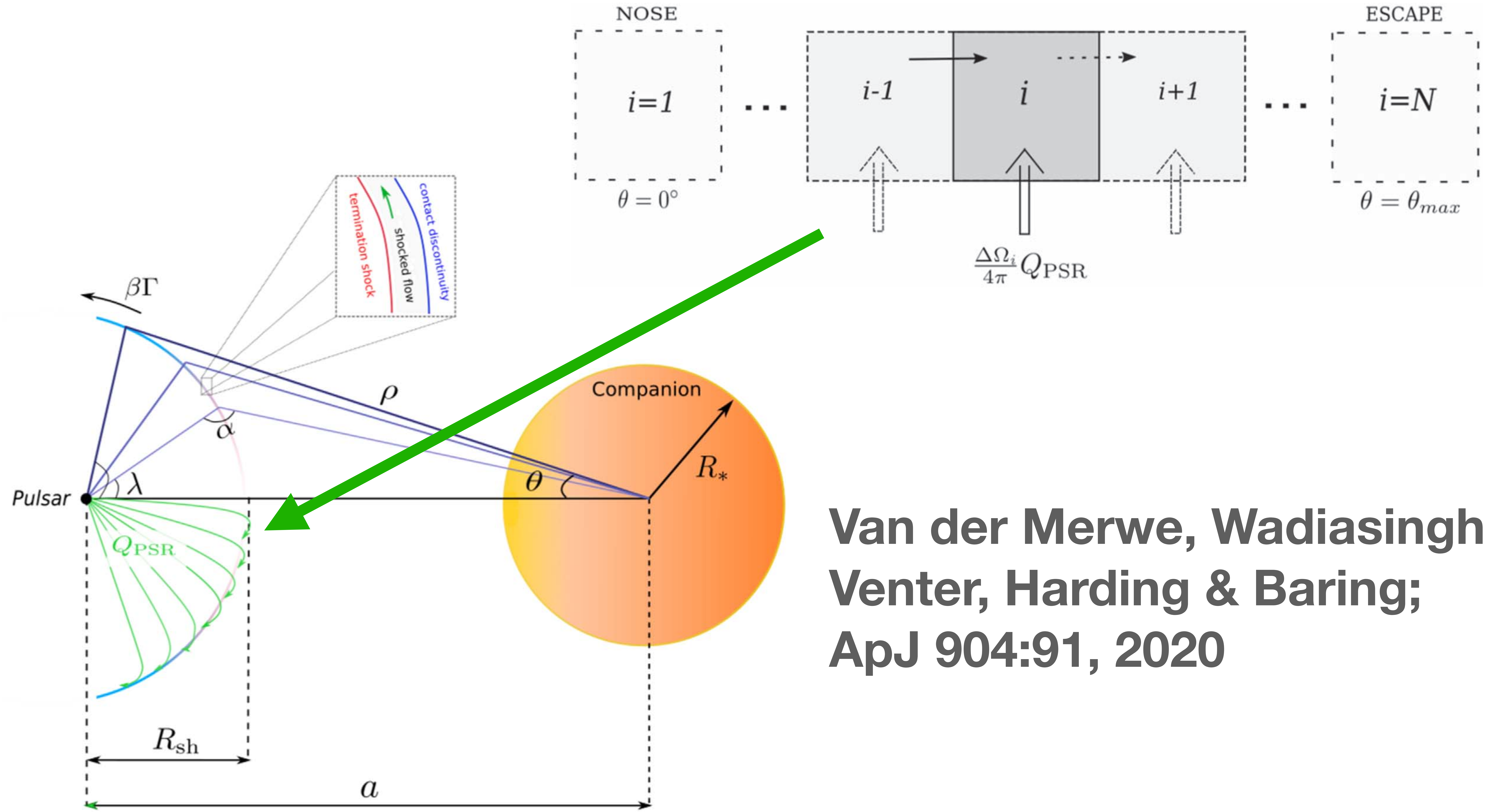

Van der Merwe, Wadiasingh, Venter, Harding & Baring; ApJ 904:91, 2020

Particle Transport (Boltzmann or Convection-Diffusion Equation)

$$\frac{\partial N_e}{\partial t} = -\vec{V} \cdot \left(\vec{\nabla} N_e \right) + \kappa(E_e) \nabla^2 N_e + \frac{\partial}{\partial E_e} \left(\dot{E}_{e,tot} N_e \right) - \left(\vec{\nabla} \cdot \vec{V} \right) N_e + Q$$

$$\Rightarrow \quad N_e = Q \tau_{eff} \qquad \tau_{eff}^{-1} = \tau_{ad}^{-1} + \tau_{diff}^{-1} + \tau_1^{-1} + \tau_2^{-1} + \tau_{rad}^{-1}$$

$$\tau_{ad} = \frac{3R_0}{c} \left[\frac{\partial \beta}{\partial \theta} + \beta \cot \theta \right]^{-1} \qquad \tau_{rad} = \frac{E_e}{\dot{E}_{e,rad}}$$

$$\tau_1 = \frac{R_0}{c\beta \tan \theta} \qquad \tau_2 = \frac{\tau_{ad}}{3} \qquad \tau_{diff} = \frac{R_0^2}{2\kappa}$$

Convection almost always dominates τ_{eff} but Doppler boosting compensates

Models

Case Study Black Widow B1957+20

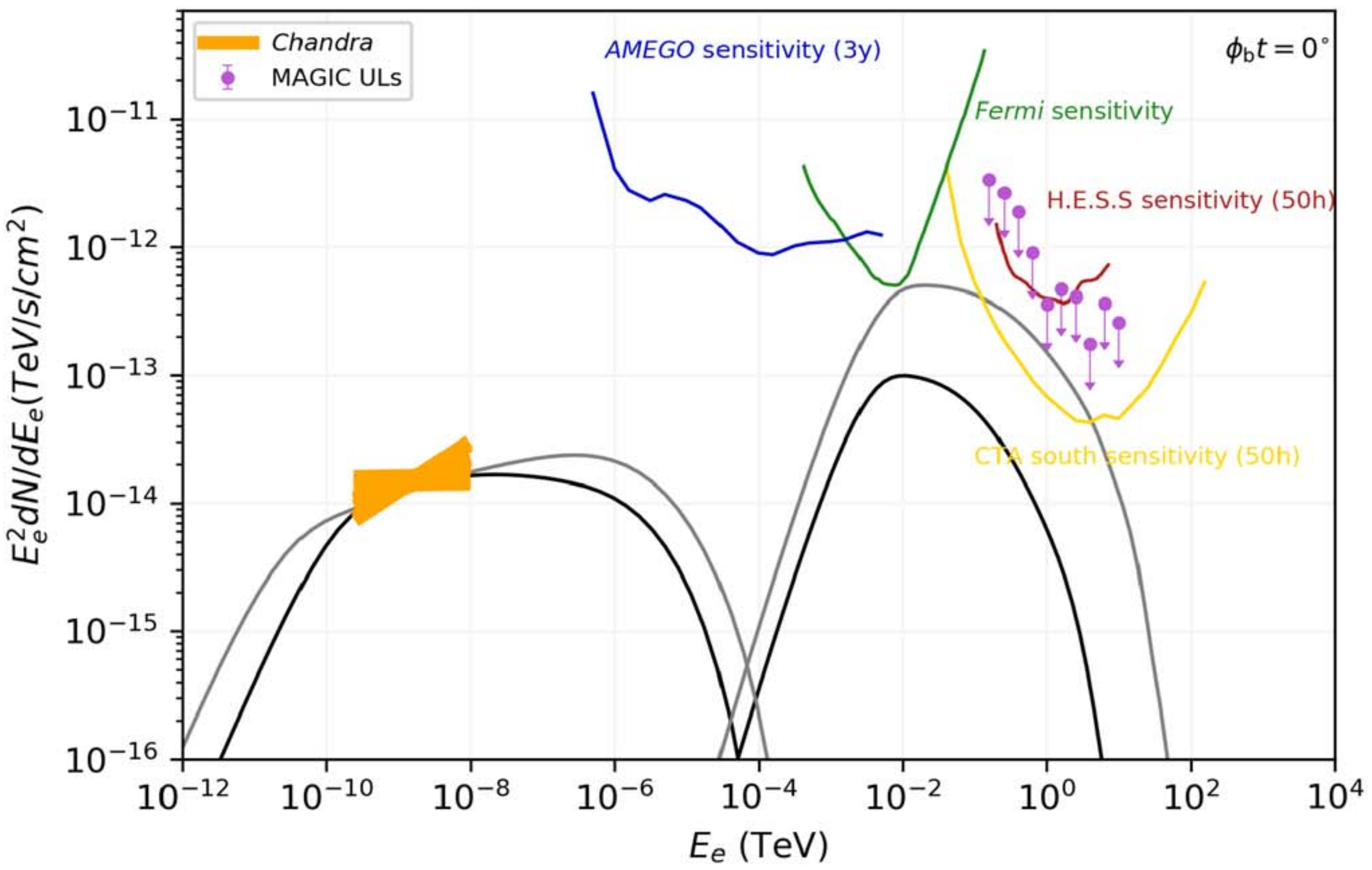

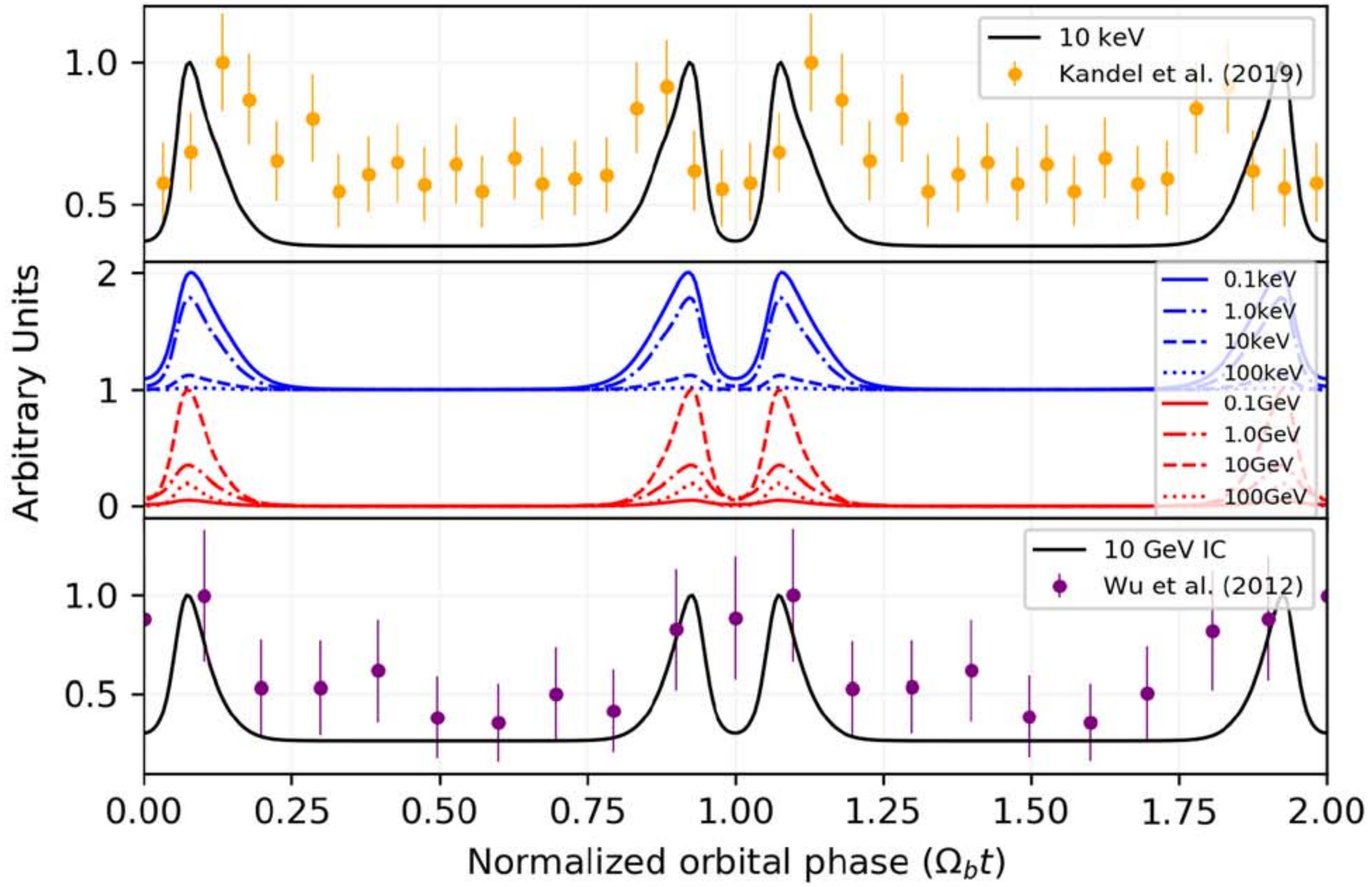

Van der Merwe, Wadiasingh, Venter, Harding & Baring;
ApJ 904:91, 2020

Models

Case Study Redback J2339–0533

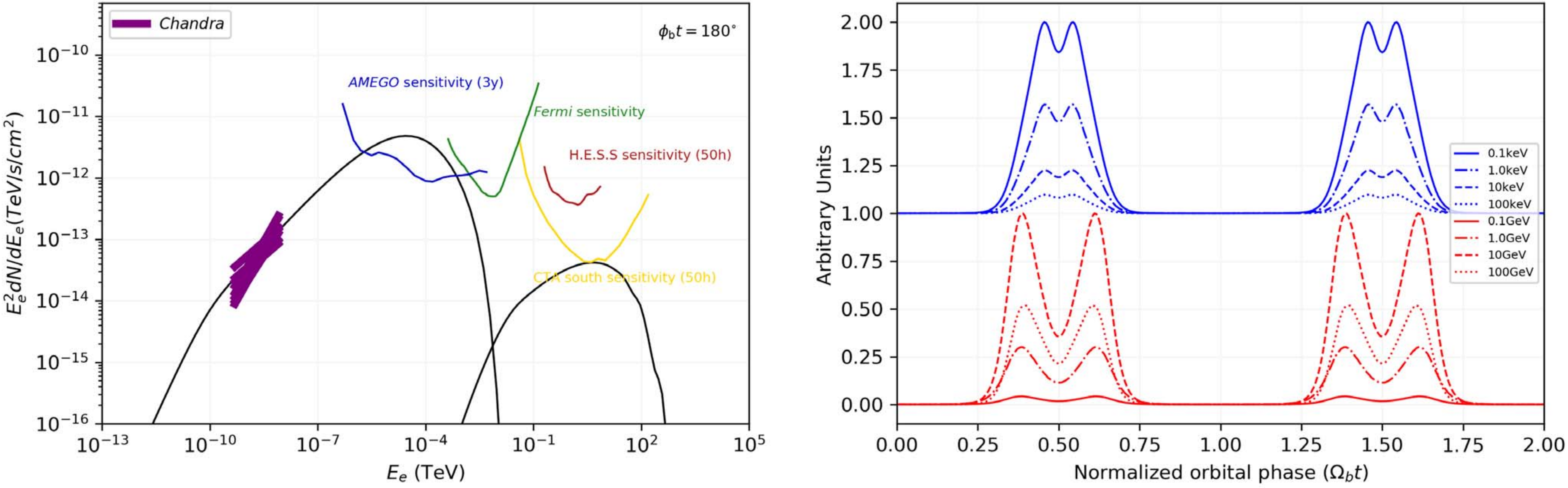

Van der Merwe, Wadiasingh, Venter, Harding & Baring;
ApJ 904:91, 2020

Model SEDs - varying injection

Case Study Redback J1723-2837

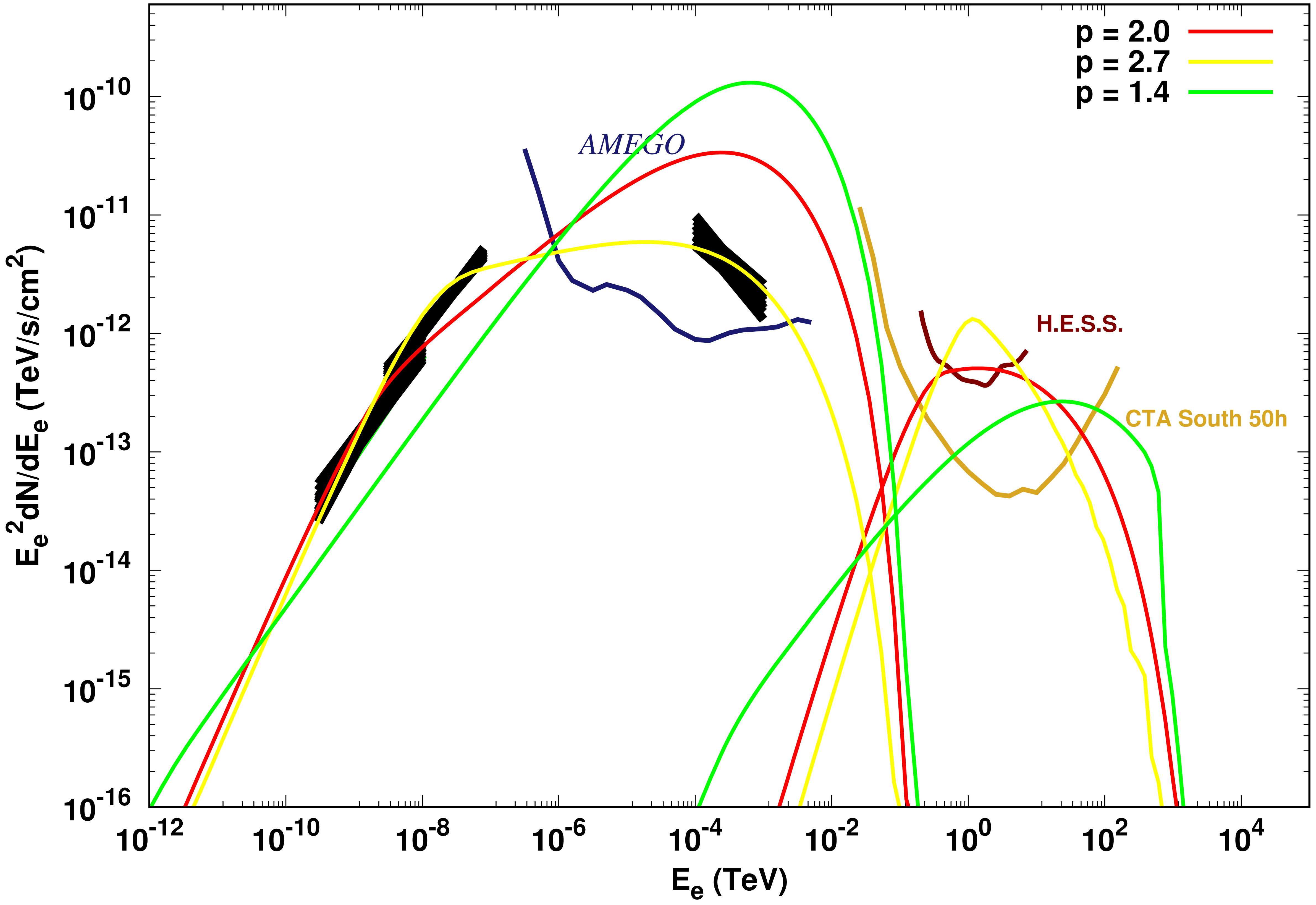

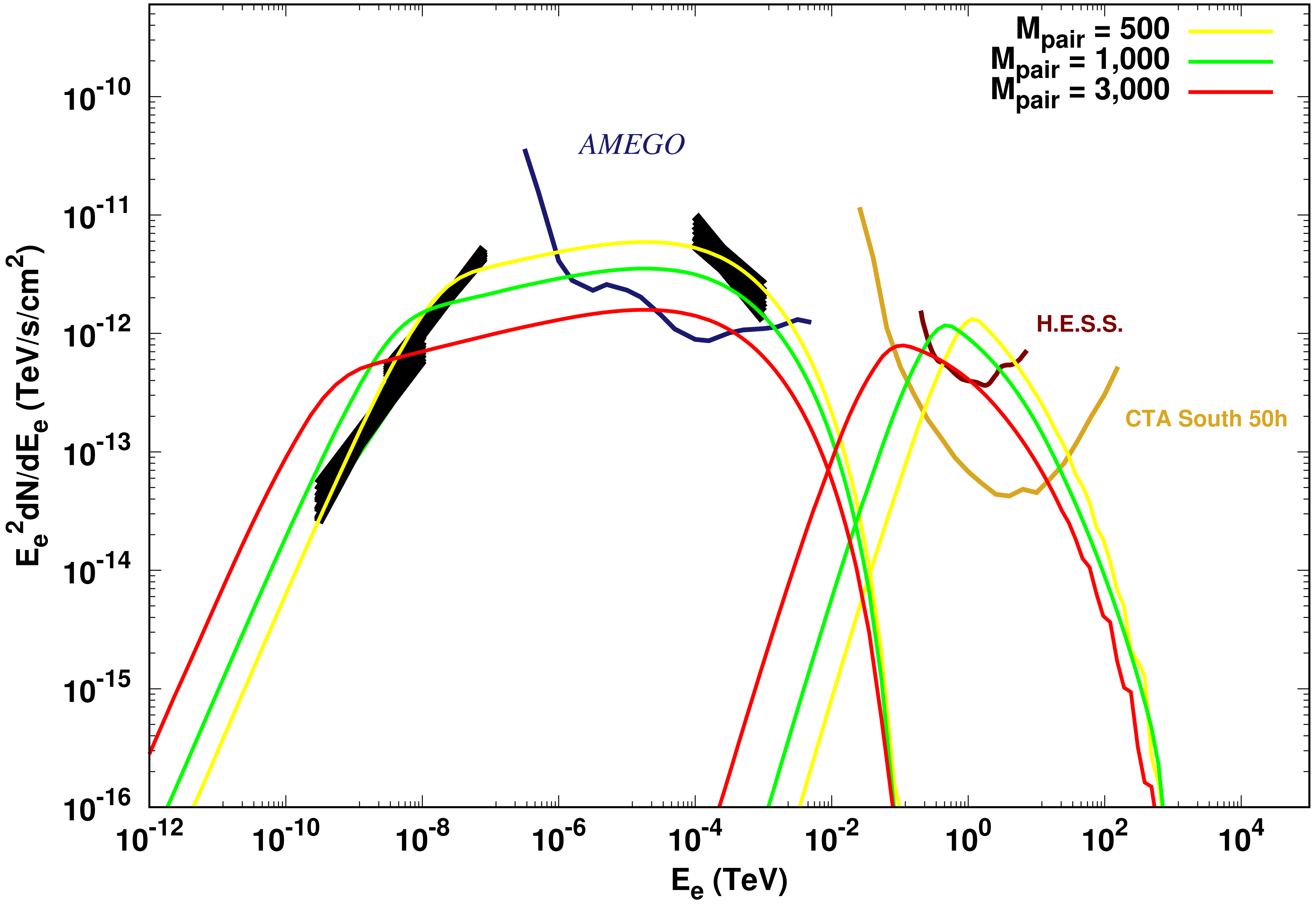

Van der Merwe, Wadiasingh, Venter, Harding & Baring;
ApJ 904:91, 2020

Model SEDs - Flaring States

Case Study Black Widow J1311–3430

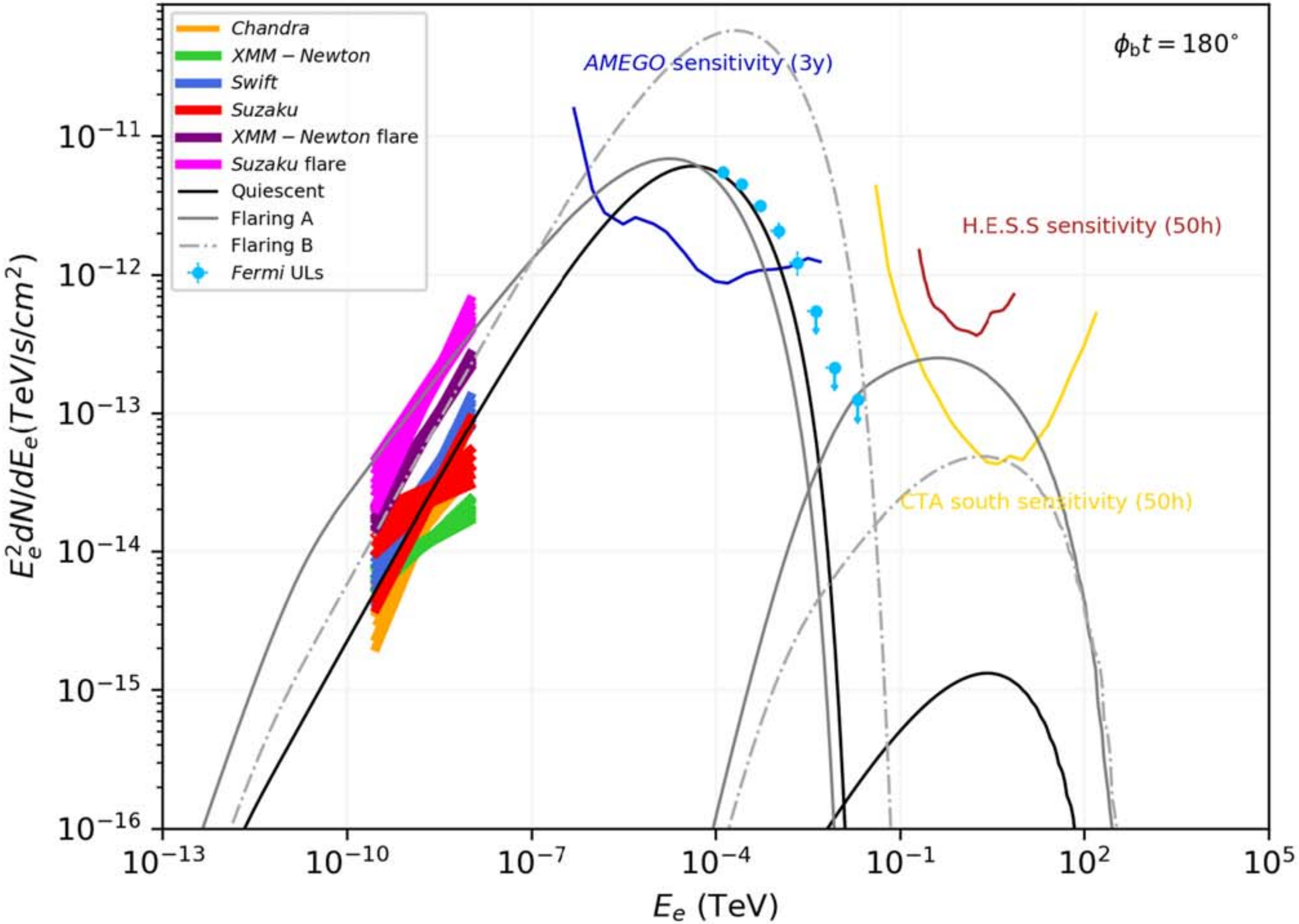

Van der Merwe, Wadiasingh, Venter, Harding & Baring; ApJ 904:91, 2020

Conclusion

- Millisecond pulsar binaries are a growing in number and are “clean” systems for understanding pulsars and pulsar winds
- We have a new multizone code which can predict SR and IC fluxes, or energy-dependent orbital modulation
- This constrains pulsar injection and particle acceleration parameters by anchoring on the X-ray
- SED could peak in the MeV — some (all?) are spiders are “gamma-ray binaries”
- Exciting for CTA and AMEGO (or any other sensitive MeV telescopes)

γγ Absorption & Pair Creation

- Although temperatures of black widow and redback companions can be high, due to their small size, absorption is insignificant except perhaps for J1311-3430 in a flaring state, where T_{eff} ~ 40000 K

- ε_0 - the energy of the outgoing VHE photon, emitted towards observer from ~ 0.2*a* near the companion

$$\tau_{\gamma\gamma}(\epsilon_0) = \int_0^\infty d\ell' \int_{\mu_-}^{\mu_+} d\mu_{\gamma\gamma}(1-\mu_{\gamma\gamma}) \int_{2/[\epsilon_0(1-\mu_{\gamma\gamma})]}^\infty d\varepsilon_s \, \frac{\partial\sigma_{\gamma\gamma}(\epsilon_0, \varepsilon_s, \mu_{\gamma\gamma})}{\partial\mu_{\gamma\gamma}} n_\gamma(\varepsilon_s) f(\mu_{\gamma\gamma}, \ell')$$

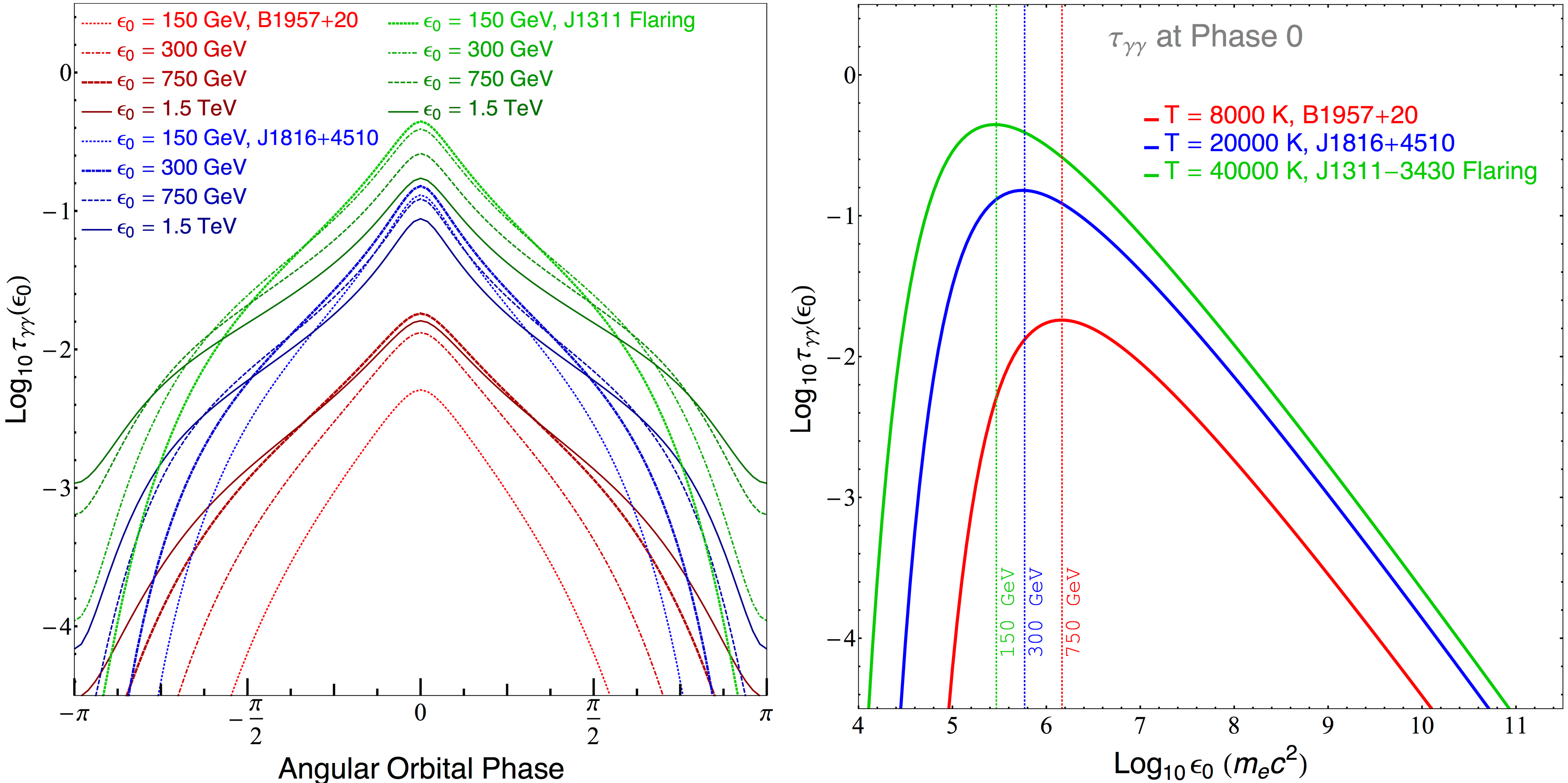

Redback J1023+0038

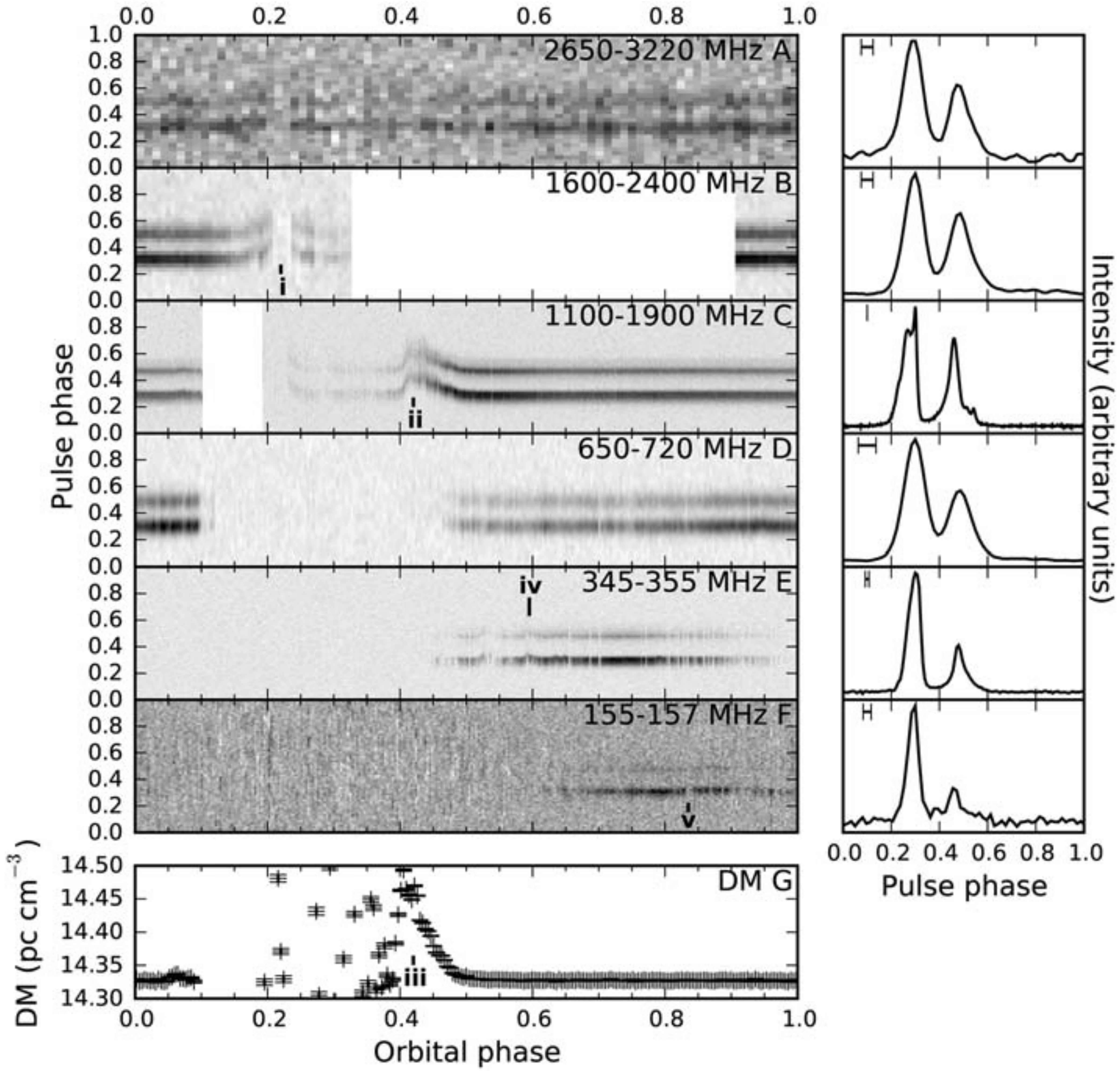

Archibald et al. (2009)

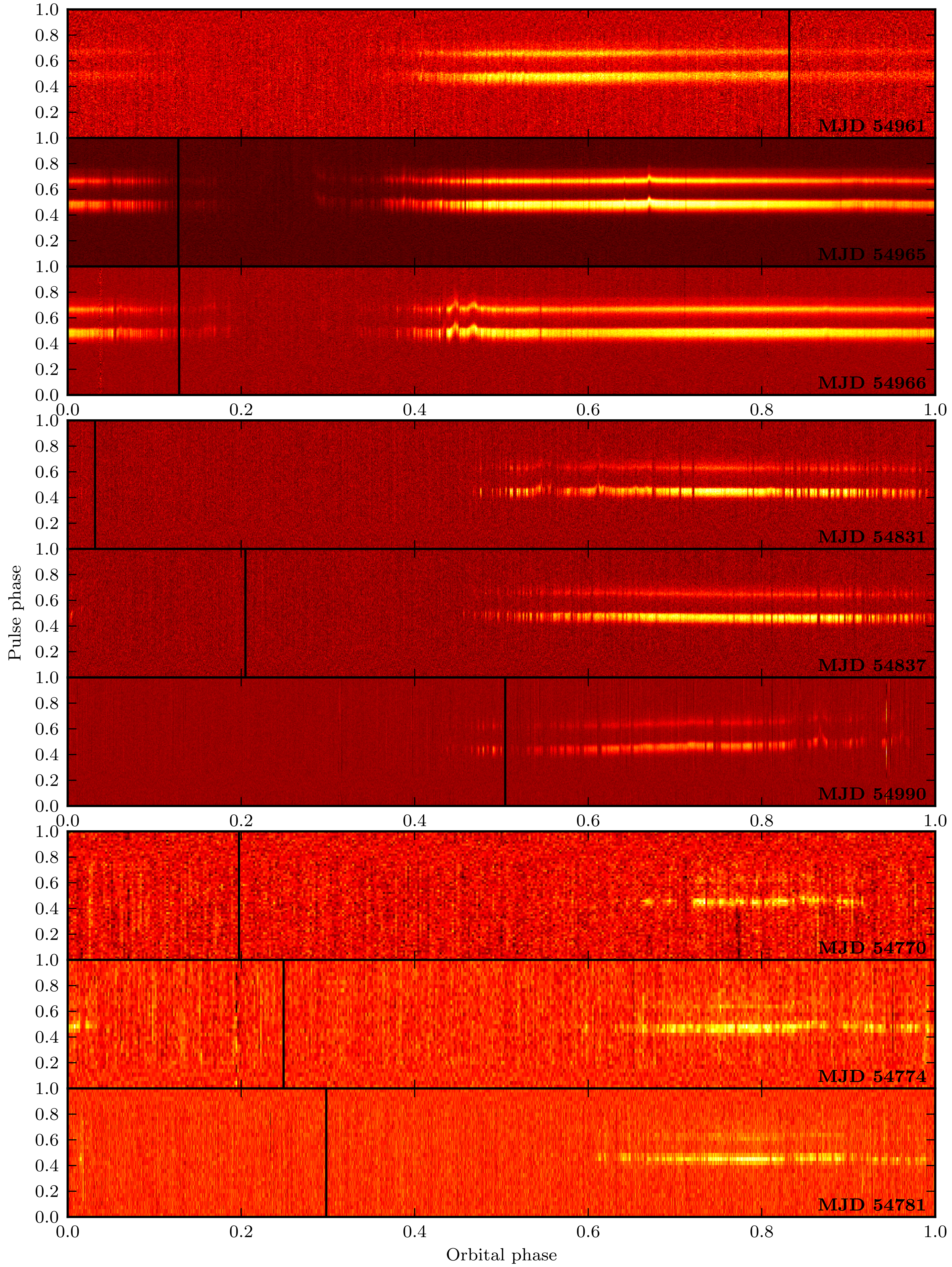

Archibald et al. (2013)

Radio Eclipses

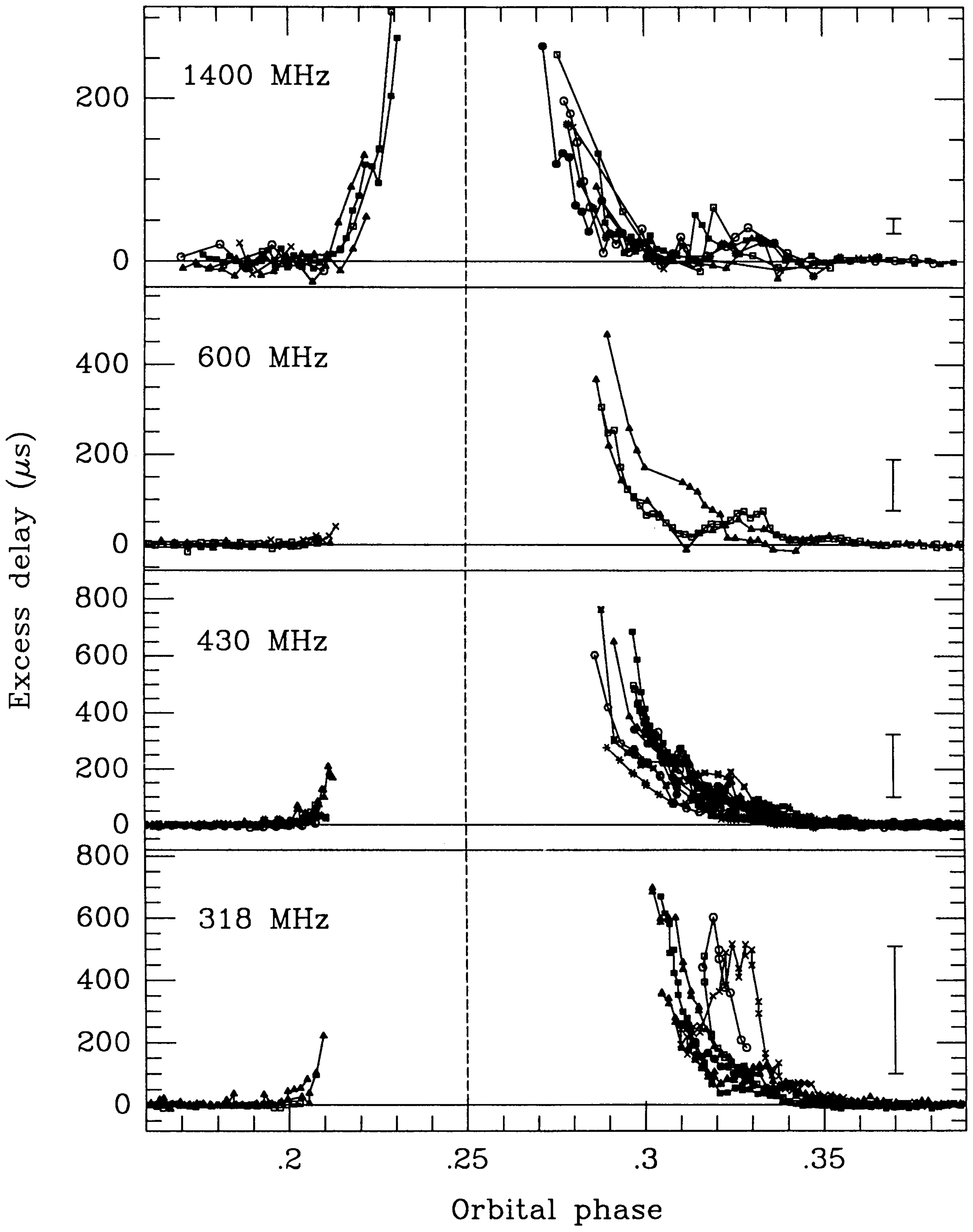

Ryba & Taylor (1991) — B1957+20

- Many black widows and redbacks show frequency-dependent radio eclipses or shrouding of the MSP over large fractions of their orbit sometimes > 50%
- Ingress-egress shrouding asymmetry tends to always decrease with higher observing frequencies ==> high frequencies probe denser wind regions closer to the shock where asymmetry due to orbital motion is lower